A Parametric Investigation of Gas-Particle Flow in a Vertical Duct

Xue Liu and Benjamin J. Glasser
Dept. of Chemical and Biochemical Engineering, Rutgers University, Piscataway, NJ 08854

DOI 10.1002/aic.10704
Published online October 17, 2005 in Wiley InterScience (www.interscience.wiley.com).

The impact of physical and process parameters on flow of gas and particles in a vertical duct has been examined. Steady-state solutions were sought to equations of continuity and motion with closures from kinetic theory and the variations of the solutions with changes in parameters were computed using a bifurcation/continuation approach. When the particles are assumed elastic, we find that the segregation of particles transits from the center to the walls with an increase in the bed width or solids load. The origin of this transition arises from the contribution of the gas-particle slip term on the pseudothermal energy transport. When the particles are inelastic, we find particles always segregate to the center of the channel, irrespective of the bed width or solids load. As we track the variation of the average solids fraction with a number of parameters, multiple steady-state solutions can be observed. Recent interest in using fluidized beds on Mars or the Moon for local production of oxygen has prompted us to examine the effect of gravity on steady fully developed flows in gas-particle fluidized beds. When the average gas velocity is held constant, the flow profiles are found to be insensitive to the magnitude of gravity if the gas flow rate is high and particles always move upward in the bed. The physical mechanism leading to this insensitivity can be traced to the automatic compensation of the gas-particle drag force to the body force. However, when the gas flow rate is low, particles move downward in the region close to the walls with high gravity, whereas this downflow is not observed under low gravity. Finally, the effects of two dimensionless numbers are investigated. It is found that the flow behaviors are not sensitive to the variation of the Reynolds number when this number is high because of a relatively small value of the gas viscous term. With an increase in the Froude number, the gas and particle velocities decrease as well as the granular temperature. © 2005 American Institute of Chemical Engineers *AIChE J,* 52: 940–956, 2006
Keywords: fluidization, bifurcation/continuation analysis, gas-particle flows, parametric analysis

Introduction

Gas fluidized bed reactors are used extensively in petroleum, chemical, pharmaceutical, agricultural, biochemical, food, electronic, and combustion processes. Fluidized bed reactors possess high heat and mass transfer coefficients as a result of excellent mixing between the gas and the solid phases.[1] There are two approaches commonly used to model the flow behavior of particles flowing with a carrier gas: the Eulerian approach[2-11] and the mixed Eulerian–Lagrangian approach.[12-15] Eulerian models, or two fluid models, treat both the gas and solid particles as a continuum, based on volume- or ensemble-averaged equations of motion. Mixed Eulerian–Lagrangian models, or discrete particle models, treat the gas phase as a continuum while computing the trajectory of each particle. The interactions between the gas phase and the particles are de-

Correspondence concerning this article should be addressed to X. Liu at liuxue@eden.rutgers.edu

scribed based on experimental and theoretical correlations. From a computational perspective, the Eulerian approach is attractive because the calculations are not limited by the number of particles in the system, which is advantageous when modeling large-scale reactors.

Equations with an averaged form have been proposed extensively in the literature.[16-19] The averaging process generates averaged quantities, such as the solid-phase stress, which require closure through constitutive relations. It is common to derive the constitutive relations for particles experiencing rapid deformation from the kinetic theory of dense gases.[20-23]

A number of theoretical studies have been performed in the last 15 years, to analyze steady, fully developed gas-particle flows in a vertical tube, using kinetic theory. To the best of our knowledge, Sinclair and Jackson[2] were the first to set up a laminar gas-laminar particle model to simulate fully developed gas-particle flows in a vertical pipe. By plotting the variation of the gas flow rate as a function of the particle flow rate for a given pressure drop, a contour map of the possible flow regimes was obtained. The performance diagrams were calculated over the whole range of cocurrent upflow and downflow, and countercurrent flow. The contour map and flow profiles qualitatively captured some important features of vertical pipe flows, such as packed beds, fluidized beds, choking, and flooding. Yasuna et al.[5] compared a large body of experimental measurements with the predictions from the model developed by Sinclair and Jackson.[2] In the paper by Yasuna et al.,[5] three types of drag coefficient closures were evaluated, and it was concluded that the flow behaviors are insensitive to the different drag force closures.

In fluidized beds, when particles are rapidly transported upward by the gas they are seen to normally segregate near the walls and the core of the reactor is occupied by a dilute region with high gas velocities.[24-27] Clearly, the flow properties, such as pressure gradient and velocity profile, are not the same as if the particles are uniformly distributed. Therefore, it is important to understand the physical mechanism responsible for this heterogeneity and to be able to predict this behavior quantitatively as a function of operating conditions (such as bed width) and the particle properties (such as the inelasticity of particles). Most previous numerical work has concentrated on determining more realistic constitutive relations and obtaining better agreement between the computational results and experimental data. The analysis of parametric influences on the flow profiles has not been developed systematically. Among a large number of physical and operating parameters in gas-fluidized beds, our study mainly focuses on six parameters: inelasticity, gravity, bed width, solids fraction, Reynolds number, and Froude number because many questions concerning the effect of these parameters on the steady-state flow profiles remain unanswered.

Inelasticity of the particles is a critical parameter for the stability of gas-particle systems. In the model of Sinclair and Jackson,[2] two coefficients are used to describe the system elasticity. One is the coefficient of particle–particle restitution, e_p, the other is the coefficient of particle–wall restitution, e_w. The value of these two coefficients ranges from zero for perfectly inelastic collisions to one for perfectly elastic collisions. A main topic of discussion on the application of the Sinclair–Jackson model is that the steady-state profiles manifest an extreme sensitivity to the coefficient of particle–particle restitution.[2-4] To eliminate this sensitivity, turbulent models have been proposed in several papers.[6-9,28] Dasgupta et al.[7,8] removed the sensitivity of the coefficient of restitution to the steady-state flow profiles by adopting a simple form for the closure of particle-phase stress. Therefore, the particle-phase stress is not dependent on the granular temperature, and the resulting equations have no reference to the coefficient of particle–particle restitution. Hrenya and Sinclair[9] described two models to investigate the combined effects of the interactions among individual particles and the interactions associated with the collective motions of particles. By adding particle turbulence contributions into the governing equations and the constitutive relation for the dissipation of pseudothermal energy, they found that the sensitivity of the system to inelastic particle–particle collisions could be substantially reduced. With respect to the laminar model, previous work has indicated that in rapid granular flows, in which particles interact by nearly instantaneous collisions, the value of granular temperature is related to the magnitude of $1 - e_p^2$.[29-31] For example, in a simple sheared system, when the effect of gravity is neglected, the granular temperature in the steady-state flow converges to a value $T = C(\gamma^2 l_0^2/\varepsilon)$, where $\varepsilon = 1 - e_p^2$ is the degree of inelasticity, l_0 is the equilibrium mean free path, γ is the shear rate, and C is a volume fraction dependent prefactor.[32] In this case, it is not surprising that the granular temperature is extremely sensitive to the coefficient of restitution when its value is close to 1, and this sensitivity is reduced as the value of the coefficient of restitution is continuously decreased.

It is well known that steady-state solutions to a laminar model are quite different from (1) time-dependent solutions to a laminar model and (2) steady-state solution to a turbulent model. The reason we choose to further examine steady-state solutions to the laminar model is that determining the effect of parameters is important for theoretically understanding the physical principles in gas-particle fluidized beds. The goal here is not to compute solutions that can be used to design or scale-up industrial risers but rather to advance the state of knowledge in this area. A long-term goal of work in this area is a full bifurcation and stability analysis for gas-fluidized beds. An investigation of steady-state flows is the first step in this regard. When carrying out bifurcation and stability analysis, it will be necessary to return to the transient model and use steady-state solutions obtained in the current paper as initial and base states. Because the base state has a critical effect on the stability analysis and the form of instability structures (bubbles, clusters, streamers), it is important to investigate parametric effects on this steady-state model. Moreover, it is likely that an understanding of the effect of parameters on steady states will give insight into the effect of the parameters on transient solutions. Although we have focused on the laminar model, we recognize that turbulent models are a powerful tool for modeling fluidized beds but, because of time averaging, they require the introduction of uncertain closures. Therefore, they do not have as strong a theoretical footing as that of laminar models.

Wang et al.[33,34] reported that for a granular flow in a channel, walls could be a source or a sink of fluctuational energy, depending on the value of e_w and e_p, where e_w describes the degree of inelasticity of collisions between particles and the walls. If $e_w < e_p$, the wall is a sink of fluctuational energy, and the granular temperature has a negative gradient toward the

walls. When $e_w > e_p$, the wall is a source of fluctuational energy, and the pseudothermal energy has a flux from the walls to the particle assembly. It is of interest to extend the study of the nature of boundaries to the gas-particle system to see their effect on the flow profiles.

Another parameter examined in this article is the gravity force, which has a significant effect on the fluidization state. Many operating parameters, such as the particle terminal velocity and the pressure gradient, vary with different values of the gravity force. An understanding of the effects of gravity on fluidized beds is important for local resource utilization on the Moon and Mars. Future missions to the Moon and Mars would likely make use of oxides in the soil and a fluidized bed is a likely candidate for processing lunar and Martian soil. Gravity is also an important parameter for the stability of fluidized suspensions. Based on the work of Gibilaro and Foscolo,[35] a significant stabilization of the fluidization process could be predicted under low gravity conditions. Compared with liquid-fluidized beds, this stabilization effect is more pronounced in gas-fluidized systems. However, the contributions of the gravity on the fully developed flow solutions of gas-particle fluidized beds have not been widely investigated.

So far the majority of theoretical studies have been confined to narrow systems. In industrial systems the width of the bed is usually many orders of magnitude larger than the particle diameter. Pita and Sundaresan[3] used the Sinclair–Jackson model to study the scale-up characteristics of pipe flows for a range of tube diameters. The occurrence of steady-state multiplicity wherein different pressure drops could be obtained for the same gas and particle flow rates was presented. They also found that for small tube diameter the pressure drop decreases rapidly as the bed diameter increases. However, when the tube diameter is sufficiently large, this trend can be reversed.

The contribution of the mean solids fraction on the stability of gas-fluidized beds has been proposed in numerous publications.[36-38] A stability analysis shows that an increase in solids fraction can suppress instabilities because the particle pressure and the solid-phase effective viscosity increase with increasing solids fraction.[39-41] The variations of the steady-state flow profiles with different average solids fractions were presented by Sinclair and Jackson[2] for a narrow gas-fluidized bed. It is of interest to extend their analysis to wider systems to see the influence of the solid fraction on the steady-state solutions.

In many articles, the governing equations were cast in dimensionless form.[2-4] Thus, dimensionless groups are introduced in the equations. In the present work, two dimensionless groups have been studied. One is the Reynolds number (Re) and the other is the Froude number (Fr). The Reynolds number can be an important parameter for the transition of flow regimes in gas-fluidized beds. Fr, which represents the ratio of inertia force to the gravity force, is also used to characterize fluidized beds.[42]

Model Equations

In this article, we examine a model that simulates the hydrodynamic behavior of gas-particle flow in a channel, assuming laminar flow for both the gas and solid phases. The geometry of the system considered is shown in Figure 1, where the gas flows from bottom to top and 2Δ is the width of the channel.

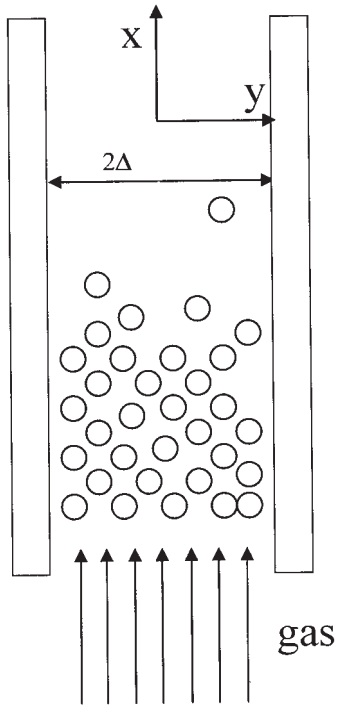

Figure 1. Bounded gas-particle flow in a fluidized bed.

The continuity and momentum balance equations for the gas and particle phases, originally proposed by Anderson and Jackson,[16] are used in the present study. For steady-state flows, these equations take the form

$$\nabla \cdot (\phi \underline{v}) = 0 \tag{1}$$

$$\nabla \cdot [(1 - \phi)\underline{u}] = 0 \tag{2}$$

$$\rho_s \phi [\underline{v} \cdot \nabla \underline{v}] = -\nabla \cdot \underline{\underline{\sigma}}_s - \phi \nabla \cdot \underline{\underline{\sigma}}_f + \underline{f} + \phi \rho_s \underline{g} \tag{3}$$

$$\rho_f (1 - \phi)[\underline{u} \cdot \nabla \underline{u}] = -(1 - \phi)\nabla \cdot \underline{\underline{\sigma}}_f - \underline{f} + (1 - \phi)\rho_f \underline{g} \tag{4}$$

where ϕ denotes the volume fraction of particles; $\underline{v}$ and $\underline{u}$ denote the local average velocities of particles and gas, respectively; ρ_s and ρ_f are the solid and gas densities respectively; g is the specific gravity force; $\underline{f}$ is the average interaction force per unit volume of bed, exerted on the particles by the gas; and σ_s and σ_f are the effective stress tensors for the particle and gas phase, respectively. Because the solid-phase stress is assumed to depend on the granular temperature, an equation representing the balance of pseudothermal energy (PTE) is required:

$$\nabla \cdot \left(\frac{3}{2} \rho_s \phi T \underline{v} \right) = -\nabla \cdot \underline{q} - \underline{\underline{\sigma}}_s^c : \nabla \underline{v} - J_{coll} - J_{vis} \tag{5}$$

Equation 5, initially proposed by Agrawal et al.,[43] represents the PTE balance, where T denotes the granular temperature that is proportional to the mean square of particle fluctuation velocity. The first term on the right-hand side represents the

diffusive transport of PTE, the second term represents the rate of production of PTE by particle–particle shear, the third term denotes the rate of dissipation of PTE through inelastic collisions, and the final term denotes the viscous damping and the production of PTE by gas-particle slip.

To solve this system, physically meaningful closures are needed to close the above equations. A form analogous to that of a Newtonian fluid is assumed for the gas-phase stress tensor:

$$\underline{\underline{\sigma}}_f = P_f \underline{\underline{I}} - \mu_{eg}\left[\nabla \underline{u} + (\nabla \underline{u})^T - \frac{2}{3}(\nabla \cdot \underline{u})\underline{\underline{I}}\right] \tag{6}$$

where P_f is the gas-phase pressure and μ_{eg} is the effective gas viscosity. In this model, we adopt the expression for μ_{eg} suggested by Sinclair and Jackson[2]:

$$\mu_{eg} = \mu_g(1 + 2.5\phi + 7.6\phi^2)(1 - \phi/\phi_{\max}) \tag{7}$$

whose value vanishes when the particles are close packed with solids fraction $\phi_{\max}$, and equals the pure gas viscosity when the bed is operated in a very dilute condition. The fluid particle interaction force is taken to have the following form[36]:

$$\underline{f} = (1 - \phi)\beta(\underline{u} - \underline{v}) \tag{8}$$

We have adopted the form for the drag coefficient β used by Anderson and Jackson[36] for the bulk of our work:

$$\beta = \frac{\phi(\rho_s - \rho_f)\, g(1 - \phi)^{1-N}}{v_t} \tag{9}$$

where v_t is the particle terminal velocity. This form is deduced from the well-known Richadson–Zaki[44] correlation and represents a convenient form for a fluidized bed at low Reynolds numbers, and is consistent with the form adopted by Sinclair and Jackson.[2] In Eq. 9, the exponent N depends on the Reynolds number based on the terminal velocity. Considering the normal flow velocity of gas-fluidized beds, a value of 3 is used in the simulations for the exponent N.[44] The evaluation of v_t was from the following correlation from Kunii and Levenspiel[1]:

$$\begin{aligned} d^* &= d\left[\frac{\rho_f(\rho_s - \rho_f)\, g}{\mu_g}\right]^{1/3} \\ v_t^* &= \left[\frac{18}{(d^*)^2} + \frac{0.591}{(d^*)^{0.5}}\right]^{-1} \\ v_t &= v_t^*\left[\frac{\rho_f^2}{\mu_g(\rho_s - \rho_f)\, g}\right]^{-1/3} \end{aligned} \tag{10}$$

To investigate the sensitivity of the results to changes in the closure for the drag coefficient, we also considered a correlation adopted by Wen and Yu[45]:

$$\beta = \frac{3}{4} C_D \frac{\phi \rho_f |v - u|}{d(1 - \phi)^{2.65}}$$

Table 1. Kinetic Theory Expressions for Particle-Phase Stress, the Pseudothermal Energy Flux, and the Rate of Dissipation Attributed to Inelastic Collisions

$$\underline{\underline{\sigma}}_s = \underline{\underline{P}}_k + \underline{\underline{P}}_c$$

$$\underline{\underline{P}}_k = \rho_s \phi T \underline{\underline{I}} - \frac{2\mu}{\eta(2 - \eta)g_0}\left[1 + \frac{8}{5}\eta(3\eta - 2)\phi g_0\right]\underline{\underline{S}}$$

$$\underline{\underline{P}}_c = \rho_s 4\eta\phi^2 g_0 T \underline{\underline{I}} - \frac{16\mu\phi}{5(2 - \eta)}\left[1 + \frac{8}{5}\eta(3\eta - 2)\phi g_0\right]\underline{\underline{S}} - \mu_b \eta\left[\frac{6}{5}\underline{\underline{S}} + (\nabla \cdot \underline{u})\underline{\underline{I}}\right]$$

$$q = -\frac{\lambda}{g_0}\left(1 + \frac{12}{5}\phi\eta g_0\right)\left[1 + \frac{12}{5}\phi\eta^2 g_0(4\eta - 3) + \frac{64}{25\pi} \times (41 - 33\eta)\phi^2\eta^2 g_0^2\right]\nabla T - \frac{\lambda}{g_0}\left(1 + \frac{12}{5}\phi\eta g_0\right) \times \frac{12}{5}\eta(2\eta - 1)(\eta - 1)\frac{d}{d\phi}(\phi^2 g_0)\frac{T}{\phi}\nabla\phi$$

$$J_{coll} = \frac{48}{\sqrt{\pi}}\eta(1 - \eta)\frac{\rho_s \varepsilon_s^2}{d} g_0 T^{3/2}$$

$$\mu = \frac{5\rho_s d\sqrt{\pi T}}{96} \qquad \mu_b = \frac{256\mu\phi^2 g_0}{5\pi} \qquad \lambda = \frac{75\rho_s d\sqrt{\pi T}}{48\eta(41 - 33\eta)}$$

$$\eta = \frac{1 + e_p}{2} \qquad g_0 = \frac{1}{1 - (\phi/\phi_{\max})^{1/3}} \qquad \underline{\underline{S}} = \frac{1}{2}[\nabla \underline{v} + (\nabla \underline{v})^T] - \frac{1}{3}\nabla \cdot \underline{v}\underline{\underline{I}}$$

$$\begin{aligned} C_D &= \frac{24}{R_{ep}}[1 + 0.15(R_{ep})^{0.687}] \quad \text{for} \quad R_{ep} < 1000 \\ C_D &= 0.44 \quad \text{for} \quad R_{ep} \geq 1000 \\ R_{ep} &= \frac{(1 - \phi)\rho_f |v - u| d}{\mu_g} \end{aligned} \tag{11}$$

The forms for particle-phase stress, the pseudothermal energy flux, and the dissipation rate of inelastic collisions, derived by Lun et al.,[20] are presented in Table 1, where P_k and P_c represent the kinetic and collisional contributions to the total particle stress tensor; g_0 is the radial distribution function taken from Johnson and Jackson[46]; μ is the viscosity of the particle phase; μ_b is the bulk viscosity for particles; λ is the pseudothermal conductivity; and S represents the deviatoric part of the particle-phase rate of deformation tensor. Our simulation shows that the second group of terms on the right-hand side of the expression for q, which denotes the contribution to the flux of the pseudothermal energy is proportional to the gradient of the particle concentration, is very small relative to the other terms even when the particle–particle restitution coefficient is <0.9. Thus this term is neglected in calculations. The fourth term on the right-hand side of Eq. 5, representing the viscous damping and production of PTE by gas-particle slip, is given by Agrawal et al.[43]:

$$J_{vis} = 3\beta T - \frac{81\phi\mu_g^2(\underline{u} - \underline{v})^2}{g_0 d^3 \rho_s \sqrt{\pi T}} \tag{12}$$

Unlike most previous work, in which the contribution of this term was not considered,[2-4] the effect of this term is investi-

gated in the present study. Our model is identical to the Sinclair–Jackson model[2] except for the inclusion of this term.

For steady, fully developed flows, the continuity equation is identically satisfied. Using ρ_s, v_t, Δ, and Δ/v_t as characteristic density, velocity, length, and time, the momentum and pseudothermal energy equations can be cast in dimensionless form:

$$-\frac{BD}{C}\frac{dp_f^*}{dx^*}-\frac{BD(1-E)}{C}f_0(u_x^*-v_x^*) - \frac{BDE}{C}+\frac{d}{dy}\left(\mu_{eg}^*\frac{du_x^*}{dy^*}\right)=0 \quad (13)$$

$$\frac{D(1-E)}{C}\left[f_0(u_x^*-v_x^*)-\phi\right]+\frac{d}{dy}\left(\frac{1}{2}f_3(T^*)^{1/2}\frac{dv_x^*}{dy^*}\right)=0 \quad (14)$$

$$\frac{d}{dy}\left(f_1T^*\right)=0 \quad (15)$$

$$\frac{d}{dy}\left(f_4(T^*)^{1/2}\frac{dT^*}{dy}\right)-D^2f_5(T^*)^{3/2}-\frac{(1-E)D}{C}3f_0T^* + \frac{D^2}{B^2}f_2(u_x^*-v_x^*)^2(T^*)^{-1/2}+f_3(T^*)^{1/2}\frac{1}{2}\left(\frac{dv_x^*}{dy^*}\right)^2=0 \quad (16)$$

where the dimensionless parameters and dimensionless variables are

$$B=\frac{\rho_s d v_t}{\mu_g} \qquad C=\frac{v_t^2}{g\Delta} \qquad D=\frac{\Delta}{d} \qquad E=\frac{\rho_g}{\rho_s}$$

$$p_f^*=\frac{p_f}{\rho_s g\Delta} \qquad u_x^*=\frac{u_x}{v_t} \qquad v_x^*=\frac{v_x}{v_t} \qquad T^*=\frac{T}{v_t^2}$$

$$\mu_{eg}^*=\frac{\mu_{eg}}{\mu_g}$$

The functions f_0 to f_5, which depend only on the solids volume fraction, are dimensionless and are given in Table 2. In the present study, the majority of the results presented will be in dimensionless form.

The boundary conditions at the wall ($y = 1$) for the particle-phase force balance and pseudothermal energy balance, originally given by Johnson and Jackson,[46] take the following forms in terms of dimensionless variables:

$$\frac{dv_x^*}{dy^*}+D\varphi' f_6 v_x^*=0 \quad (17)$$

$$\frac{dT^*}{dy^*}-D\varphi' f_7(v_x^*)^2+D(1-e_w^2)f_8T^*=0 \quad (18)$$

where φ' is the specularity coefficient whose value ranges from zero if the collisions between the walls and particles are specular to unity if the incident particles are scattered diffusely, representing the roughness of the walls; f_6–f_8 are dimensionless functions defined in Table 2. In most theoretical studies on gas-particle fluidized beds, a no-slip or (stress) free boundary condition is applied to the gas phase. This is true for the point velocity of the gas at the walls. However, the gas velocity appearing in the equations of motion is not this, but some suitable average. Therefore, an appropriate boundary condition for the gas velocity at the walls is a subject of debate. The boundary condition representing the force balance of gas phase originally proposed by Sinclair and Jackson[2] was used in the bulk of this work:

$$\mu_{eg}^*\frac{du_x^*}{dy^*}+\frac{BDG(1-E)}{C}\frac{\phi}{\phi_{\max}}f_0(u_x^*-v_x^*)+\frac{BDG}{C}\frac{\phi}{\phi_{\max}}\frac{dp_f^*}{dy^*} + 2G\frac{\phi_{\max}}{\phi}T^*u_x^*=0 \quad (19)$$

where G is a dimensionless variable related to the thickness of a layer adjacent to the wall in which we calculate the force balance. To study the effect of the gas boundary conditions on flow profiles, simulations based on no-slip and free gas-phase boundary conditions have also been carried out. We found under our physical situation the flow profiles are not sensitive to the gas-phase boundary conditions. Only a small difference can be observed in the region close to the walls (see Figure 2). However, to keep consistent with equations with averaged forms, the expression proposed by Sinclair and Jackson[2] was used in the following simulations. It is found that the governing equations along with the boundary conditions admit the following symmetry:

$$u_x^*(y)=u_x^*(-y) \qquad v_x^*(y)=v_x^*(-y)$$

$$\phi^*(y)=\phi^*(-y) \qquad T^*(y)=T^*(-y)$$

Table 2. Dimensionless Functions f_0–f_8

$$f_0=\phi(1-\phi)^{1-N}$$

$$f_1=\phi(1+4\eta\phi g_0)$$

$$f_2=\frac{81\mu_{eg}^2}{g_0\sqrt{\pi}}\phi$$

$$f_3=\frac{2+\alpha}{3}\left[\frac{5\sqrt{\pi}}{48g_0\eta(2-\eta)}\left(1+\frac{8}{5}\eta\phi g_0\right)\left(1+\frac{8}{5}\eta(3\eta-2)\phi g_0\right)+\frac{16}{5}\eta\frac{\phi^2 g_0}{\sqrt{\pi}}\right]$$

$$f_4=\frac{25\sqrt{\pi}}{16\eta(41-33\eta)g_0}\left\{\left(1+\frac{12}{5}\eta\phi g_0\right)\left[1+\frac{12}{5}\eta^2(4\eta-3)\phi g_0\right]+\frac{64}{25\pi}(41-33\eta)(\eta\phi g_0)^2\right\}$$

$$f_{4h}=\frac{25\sqrt{\pi}}{16\eta(41-33\eta)g_0}\left(\frac{1}{\phi}+\frac{12}{5}\eta g_0\right)\frac{12}{5}\eta(2\eta-1)(\eta-1)\frac{d}{d\phi}(\phi^2 g_0)$$

$$f_5=\frac{48}{\sqrt{\pi}}\eta(1-\eta)\phi^2 g_0$$

$$f_6=\frac{\sqrt{3}}{3}\frac{\pi\phi g_0}{\phi_{\max}f_3}$$

$$f_7=\frac{\sqrt{3}}{6}\frac{\pi\phi g_0}{\phi_{\max}f_4}$$

$$f_8=\frac{\sqrt{3}}{4}\frac{\pi\phi g_0}{\phi_{\max}f_4}$$

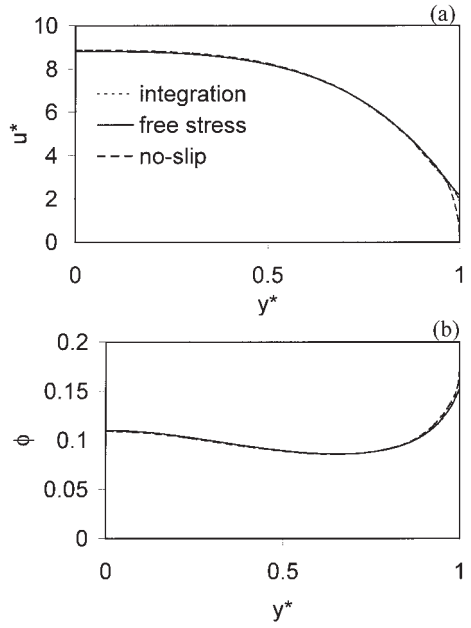

Figure 2. Effects of gas boundary conditions on the flow profiles.

$e_p = 1$, $\phi = 0.1$. (a) gas velocity profile; (b) solids fraction profile.

Thus, a relevant boundary condition at $y = 0$ can be written as

$$\frac{du_x^*}{dy^*} = 0 \qquad \frac{dv_x^*}{dy^*} = 0 \qquad \frac{dT^*}{dy^*} = 0 \tag{20}$$

The base physical parameters used in this model are listed in Table 3, representing cocurrent upflow of 400 μm diameter particles in air at 500°C and 6.5 atmosphere in a narrow channel. Equations 13–20 describe a steady-state gas-particle laminar flow in a channel.

The above model consists of four ordinary differential equations and four unknowns (u, v, ϕ, and T), subject to two point boundary conditions. Equation 15 can be rewritten as an algebraic equation to provide an explicit relation between ϕ and T. This eliminates one unknown and leaves only three differential equations and three unknowns. A numerical method based on the orthogonal collocation approach[47] is set up to obtain the solutions for the base state. Another numerical scheme, that is, a second-order finite-difference method is also used to ascertain the correctness of the solutions. Preliminary results confirm that both numerical methods yield the same solutions.

Table 3. Basic Simulation Parameters

d	Particle diameter	400 μm
v_t	Particle terminal velocity	1.37 m/s
μ_g	Viscosity of gas	0.00004 kg ms^{-1}
ϕ_{max}	Maximum solid volume fraction	0.65
ρ_g	Gas density	3 kg/m^3
ρ_s	Solid density	1500 kg/m^3
N	Richardson–Zaki number	3
g	Gravitational acceleration	9.81 N/kg
2Δ	Bed width	4 cm
e_w	Particle–wall restitution coefficient	0.9
φ'	Specularity coefficient	0.5

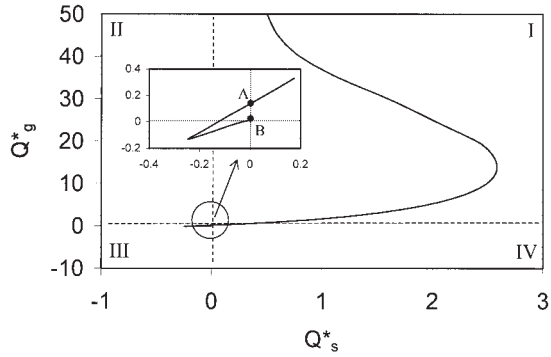

Figure 3. Gas flow rate vs. solid flow rate at a constant pressure gradient.

$dp^*/dx^* = -0.4$; $e_p = 1$; $D = 500$; $2\Delta = 40$ cm. All other parameters are given in Table 3.

From the simulation, it is found that multiple solutions can be obtained with different initial guesses. To find all possible solutions and track the variation of the solutions with different parameters, we make use of a bifurcation analysis and continuation approach with AUTO 86 software.[48] The calculation procedure of the continuation approach involves the following steps. First, input a steady-state solution into the AUTO 86 software as the initial state. Then the software calculates the solution branches as a function of the chosen parameter as other physical parameters are kept unchanged. In the present work, the continuation is carried out based on two different algorithms. The first is examining the variation of the solids fraction amplitude, $\phi_{max} - \phi_{min}$, with a chosen parameter, which requires calculating the differential form of Eq. 15 with two constraints, $d\phi/dy = 0$ at the center and the average solids fraction across the channel is a constant. The second involves examining the change of the average solids fraction with a chosen parameter. This requires rewriting Eq. 15 in an algebraic form:

$$f_1 T^* = C_1 \tag{21}$$

and calculating the steady-state solutions in terms of the coefficient C_1.

In previous work, simpler models have been used to simulate the hydrodynamics in gas-fluidized beds,[16,36,39-41] where the solids-phase stress was not dependent on the granular temperature. Therefore, the PTE balance equation was not required. To investigate the contribution of the PTE equation on bounded gas-particle flows, the model, originally proposed by Glasser et al.[41] for unbounded flows, is examined in a channel with no-slip boundary conditions for both gas and particle phases. Although the gas and solid velocity profiles computed using the model in Glasser et al.[41] share similar features to those computed using the present model, the solids fraction is always uniform across the bed because the equation representing the momentum balance in the lateral direction can be simplified as ϕ = constant. Clearly, the uniform solids fraction profile is unrealistic for bounded channel flows, so the PTE equation is indispensable for bounded flows.

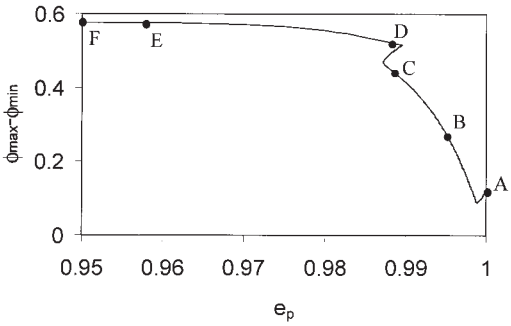

Figure 4. Variation of the solids fraction amplitude, $\phi_{max} - \phi_{min}$, with e_p.

$\phi = 0.2$. Parameters are given in Table 3.

Results and Discussion

An overall view of possible flow regimes of gas-particle flow in a vertical channel is shown in Figure 3. This is examined by plotting the variation of dimensionless gas volume flow rate Q_g^* as a function of the dimensionless solid volume flow rate Q_s^* for a given value of the pressure drop, where $Q_s^* = Q_s/(\Delta^2 v_t)$ and $Q_g^* = Q_g/(\Delta^2 v_t)$. The curve in the first quadrant represents cocurrent upflow. The curves in the second and third quadrants describe countercurrent flow and cocurrent downflow, respectively. When the gas flow rate is reduced in the first quadrant, the solid flow rate increases initially, passes through a maximum, and then decreases. After crossing the axis into the second quadrant, the solids flow rate continues decreasing, then passes through a minimum in the third quadrant and moves back toward positive values of the solid flow rate. Figure 3 clearly shows the existence of multiple solutions, which means that for a given solid flow rate, the system can have more than one steady-state solution. This kind of contour map and steady-state multiplicity were also reported by Sinclair and Jackson.[2] It is interesting to note that for a zero value of the solid flow rate, the gas flow rate has two values, where point A represents a dilute fluidized state, whereas point B represents a fluidized state close to the maximum particle packing. In this work, we have focused on solutions in the first quadrant, which corresponds to cocurrent upflow.

The contribution of particle inelasticity on granular flows and gas-particle flows has been discussed in a number of papers.[9,29,30] Figure 4 shows the solids fraction amplitude, $\phi_{max} - \phi_{min}$, as a function of the coefficient of particle–particle restitution. When e_p is close to 1, the solids fraction amplitude is very sensitive to this parameter. However, when its value is <0.985, a plateau can be observed, indicating that e_p has little effect on the flow structures. To better understand the structures of the branches in the continuation map, the flow profiles for points A, B, C, D, E, and F are plotted. Figure 5 shows the variation of the solids fraction, granular temperature, and gas and solid velocities within the fluidized bed for points A, B, E, and F. When elastic collisions between particles in fluidized beds are assumed (point A, $e_p = 1$), there is a plateau of low solids density in the center region and a relatively large concentration of particles near the walls. The granular temperature increases slightly when moving away from the center, passes through a maximum, and then decreases rapidly near the walls. The relation of the solids fraction and the granular temperature is predicted in terms of Eq. 15 that the solid concentration should be small in regions where the granular temperature is large, and vice versa.

The variation of gas and solid velocities is shown in Figures 5c and 5d, respectively. For the elastic case, both velocities are higher at the center and lower at the walls. The velocity difference between the gas phase and solid phase is associated with the well-known drag force. It has been shown that the drag force plays a key role in the formation of heterogeneous flow structures in gas-particle fluidized beds when collisions between particles are ideal.[14] This "core–annular" flow structure in gas-particle fluidized beds has been discussed in many papers and is typically observed in fast gas-fluidized beds.[25,49-52] However, when collisions between particles are slightly inelastic (point B, $e_p = 0.995$), the flow profiles exhibit a different structure. Under this condition, there is a segregation of particles near the center and a dilute region near the walls (Figure 5a). This type of flow structure has been observed

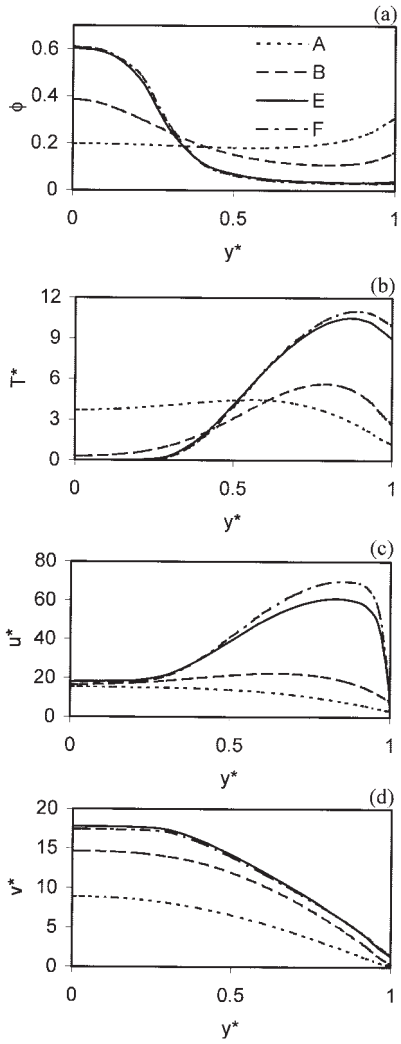

Figure 5. Effect of the coefficient of particle–particle restitution on gas-particle channel flow.

$\phi = 0.2$. (a) Solids fraction profile; (b) granular temperature profile; (c) gas velocity profile; (d) solid velocity profile (points A, B, E, and F are given in Figure 4).

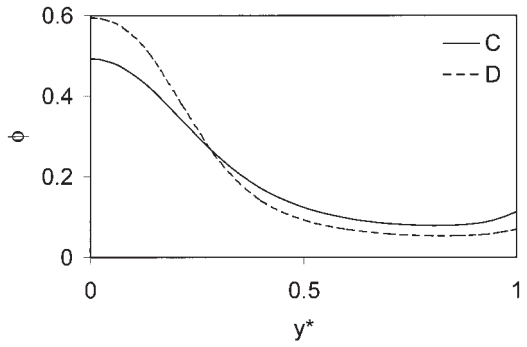

Figure 6. Solids fraction profiles corresponding to points C and D in Figure 4.

$\phi = 0.2$. Parameters are given in Table 3.

in computer simulations of gas-fluidized beds.[2,12] To the best of our knowledge, this flow structure has not been experimentally observed in gas-fluidized beds, although is has been observed in liquid-fluidized beds.[53,54] The gas-phase velocity initially remains a constant value when moving away from the center, passes through a maximum corresponding to the maximum in the granular temperature profile, and then decreases quickly near the walls (Figure 5c). This relation between the granular temperature and the superficial gas velocity has been observed in experiments.[55,56] When $e_p = 0.995$, the solid velocity has a maximum value in the center and decreases when moving toward the walls (Figure 5d). When the system becomes more inelastic (point E, $e_p = 0.96$; point F, $e_p = 0.95$), the segregation of particles is more pronounced and a plug flow with maximum solids fraction can be seen near the center. Therefore, using this laminar model core–annular solutions cannot be obtained unless the restitution coefficient is equal to unity. In Figures 5c and 5d, the relative velocity between gas and solids is quite large in the region close to the walls if collisions between particles are inelastic, which is attributed to the segregation of particles. For inelastic cases, most particles segregate in the center and there is a dilute region close to the walls. Because the drag coefficient decreases with a decrease in solids fraction, the value of the drag coefficient is much larger in the center than that close to the walls. At the same time, the gas–solids relative velocity increases from the center to the walls. Similar flow profiles were also obtained by Sinclair.[57]

Scrutiny of Figures 4 and 5 reveals that the sensitivity to the coefficient of restitution occurs only when e_p is close to 1. When the gas-particle system transits from an elastic case to a slightly inelastic one, the particles start to migrate from the walls to the center. When the solids concentration is equal at the center and the walls, the solids fraction amplitude goes through a minimum (see Figure 4, $e_p = 0.998$). With a further decrease in e_p, the solids fraction becomes higher at the center than at the walls, leading to an increase in the solids fraction amplitude. Once e_p is <0.985, a solids fraction close to the packed bed limit is observed at the center, indicating that a maximum solids fraction amplitude is approached. With a further decrease in e_p, the gas-particle flow profiles are not sensitive to this parameter. Another interesting phenomenon observed in the continuation is that the profile of solids fraction amplitudes has an "S" form bifurcation diagram when e_p is between 0.990 and 0.986, indicating the existence of multiple solutions for a fixed set of physical parameters. To better understand this bifurcation diagram, the solids fraction profiles are plotted for points C and D ($e_p = 0.988$). Figure 6 shows that the solution branch corresponding to D–E represents a state of maximum solids fraction at the center, whereas the solution branch corresponding to B–C represents a transition process of particle segregation from the walls to the center.

By examining the continuation map and the solids fraction profiles (see Figures 4 and 5), we can see that a transition from "core–annular" structure to center segregation of particles occurs when e_p decreases from 1 to 0.99, and with a further decrease in e_p the flow profiles are not sensitive to this parameter. This is in agreement with the results of Goldhirsch[32] that the granular temperature is related to $1 - e_p^2$. It is clear that when e_p is changed from 0.99 to 0.999, the value of $1 - e_p^2$ is changed tenfold. However, when e_p is changed from 0.95 to 0.96, the value of $1 - e_p^2$ varies by only 1.24-fold. Accordingly, it is not surprising that the extreme sensitivity exists in the gas-particle flow when e_p is close to 1, and this sensitivity is reduced when the system becomes more inelastic.

From Figure 5, it can be observed that the granular temperature near the walls increases as e_p decreases, indicating that the flow structures have a potential to switch from a situation where the wall behaves as a sink of PTE to a source of PTE. This variation can be related to the value of the coefficient of particle–wall restitution (e_w). The effect of e_w on the solids fraction and granular temperature is shown in Figure 7. It can be seen that e_w plays a small role in the solids fraction profiles. Small variations are obtained only in the region near the walls when e_w is increased from 0.6 to 0.99. The impact of e_w on the granular temperature is more pronounced. When e_w is sufficiently large, the wall is a source of fluctuational energy. The value of granular temperature increases on moving toward the

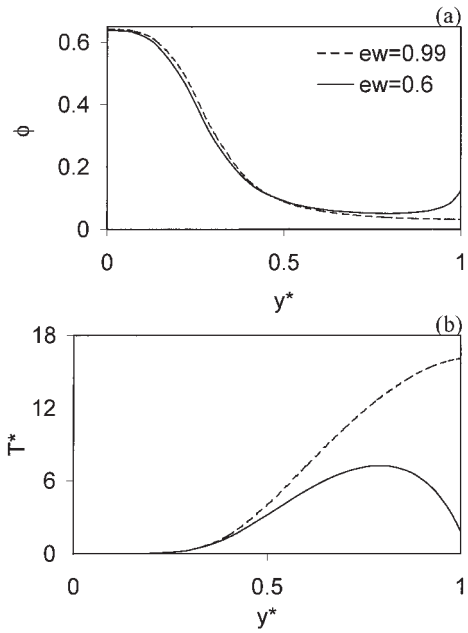

Figure 7. Effect of the particle–wall restitution coefficient on gas-particle channel flow.

$\phi = 0.25$, $e_p = 0.96$. (a) Solids fraction profile; (b) granular temperature profile.

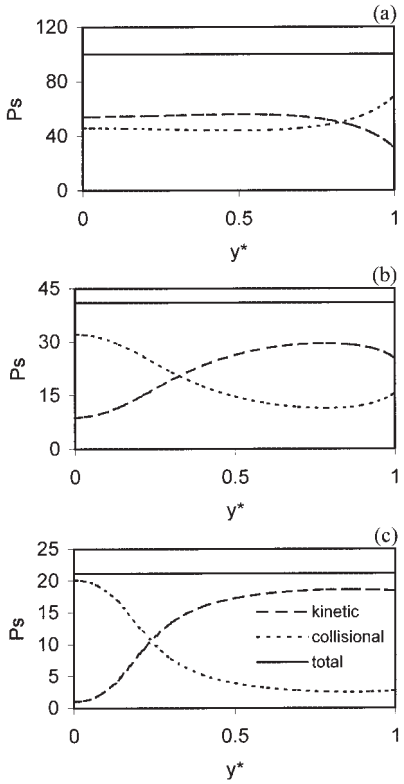

Figure 8. Particle pressure profiles across the bed.

$\phi = 0.1$. (a) $e_p = 1$; (b) $e_p = 0.99$; (c) $e_p = 0.96$.

walls from the center. If e_w is small, however, the wall is a sink of fluctuational energy, and the granular temperature decreases near the walls. Because the velocity profiles exhibit only a small difference when e_w changes from 0.99 to 0.6 and they are quite similar to the case of $e_p = 0.96$ in Figures 5c and 5d, the results are not shown here. Based on these results, it is clear that the solids fraction profiles are not sensitive to the different values of e_w.

In the kinetic theory closures, if the frictional contribution is neglected, the particle pressure is composed of two terms, the kinetic part and collisional part.[20] To the best of our knowledge, the distribution of the particle pressure across the bed has not been examined for continuum models for bounded gas-particle flows. Figure 8 shows the effect of the coefficient of restitution (e_p) on the distribution of solids-phase pressure through the channel. It is found that the magnitude of the total particle pressure strongly depends on the value of coefficient of restitution. The increase in the total particle pressure with an increase in e_p can be attributed to the fact that the system loses less energy as e_p increases, and the particles move faster and have a higher chance to collide with each other than in systems that are characterized by a lower coefficient of restitution. Similar results were reported by Liss and Glasser[58] for a sheared granular flow. In Figure 8, it can be seen that the profile of the collisional contribution has a transition from a high value at the walls to a high value in the center when e_p is decreased from 1 to 0.96. This indicates that the distribution of particles should also have a transition with a decrease in e_p because the value of the collisional pressure is proportional to the solids fraction. The transition of the kinetic contribution, however, is opposite with a decrease in e_p. Its maximum value switches from the center to the walls when e_p is decreased from 1 to 0.96. It is clear that large fluctuational velocity is expected to be seen in the region of high kinetic pressure. Because the granular temperature is proportional to the mean square of fluctuational velocity, high kinetic pressure should correspond to a large granular temperature and a small solids fraction. It is important to note that the transitions of the collisional pressure and kinetic pressure occur when e_p is decreased from 1 to 0.99. A further decrease in e_p from 0.99 to 0.96 just makes this transition increasingly more pronounced. Therefore, it is clear that there is a relation between the sensitivity to e_p and the transition of the solids-phase pressure.

The second parameter examined in this article is gravity (g). Figure 9 shows the variation of solids fraction amplitude, $\phi_{\max} - \phi_{\min}$, as a function of gravity. The variation of the solids fraction amplitude with g is gradual and smooth, indicating that the flow structures are fairly insensitive to changes in this parameter. To further study the effect of g, the flow profiles of solids fraction, granular temperature, and gas and solid velocities are examined for $g = 9.81$ m/s^2 and $g = 1$ m/s^2, respectively. When the pressure drop is held constant, the gas and solid flow rates substantially increase with a decrease in gravity. However, a more appropriate comparison for a fluidized bed reactor is to keep the residence time or velocity of the gas a constant to complete reactions appropriately. Therefore, in the flow profile plots, we keep the average gas-phase velocity a constant by reducing the pressure drop across the bed as gravity is decreased. The dimensional equations are used to analyze the effect of gravity in that the dimensionless model uses the solid terminal velocity as characteristic velocity and the solid terminal velocity is related to gravity. In Figure 10, elastic collisions between particles are assumed, so the "core–annular" flow structure is obtained. It can be seen that in this case the flow structures for constant average gas velocity are insensitive to the different values of gravity. The profiles of solids fraction and granular temperature are quite similar when g changes from 9.81 to 1 m/s^2, except that the particle segregation near the walls is slightly more pronounced when the gravity is higher. The gas and solid velocity profiles are also similar as g changes except that the solids velocity in the lower gravity case is slightly smaller.

The similarity of flow profiles with the variation of g is related to the compensation between the body force and the

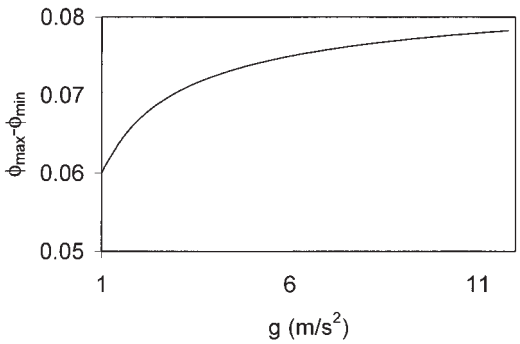

Figure 9. Variation of the solids fraction amplitude, $\phi_{\max} - \phi_{\min}$, with gravity.

$\phi = 0.1$, $e_p = 1$.

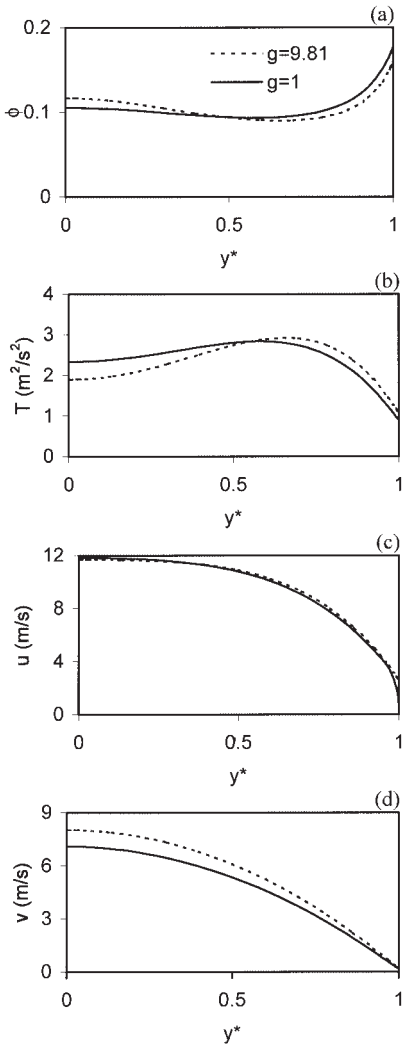

Figure 10. Effect of gravity on gas-particle channel flow for a high gas velocity.

u_g = 10m/s, e_p = 1, ϕ = 0.12. (a) Solids fraction profile; (b) granular temperature profile; (c) gas velocity profile; (d) solid velocity profile.

drag force, and the fact that we have kept the average gas-phase velocity a constant. In a lower gravity system, although the body force—driving particles downward—is small, the drag force, which keeps the particles in suspension, is also relatively small. To better illustrate this relation, the difference between the magnitude of the drag force and the magnitude of the gravity force is plotted in Figure 11. It can be seen that the difference between the drag force and the gravity force changes only slightly when the gravity changes nearly one order of magnitude. This result indicates that for a fluidized bed system with a high gas velocity the effect of changing the gravitational force can be automatically eliminated by the corresponding change of the drag force. Therefore, the base states are not sensitive to the parameter g. From Figure 10, it can be seen that particles always move upward under both high and low gravity situations when there is a high gas velocity. However, many riser flows operate with solids recirculating downward in the annular region close to the walls while still maintaining a

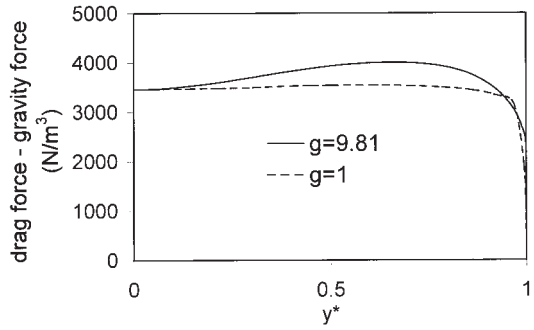

Figure 11. Profiles of drag force minus gravity force.

u_g = 10 m/s, e_p = 1, ϕ = 0.12.

positive net solids flux. Because the gravity causes the solids to flow downward, it is interesting to see the effect of the gravity on this flow regime.

Figure 12 shows that the effect of the gravity becomes

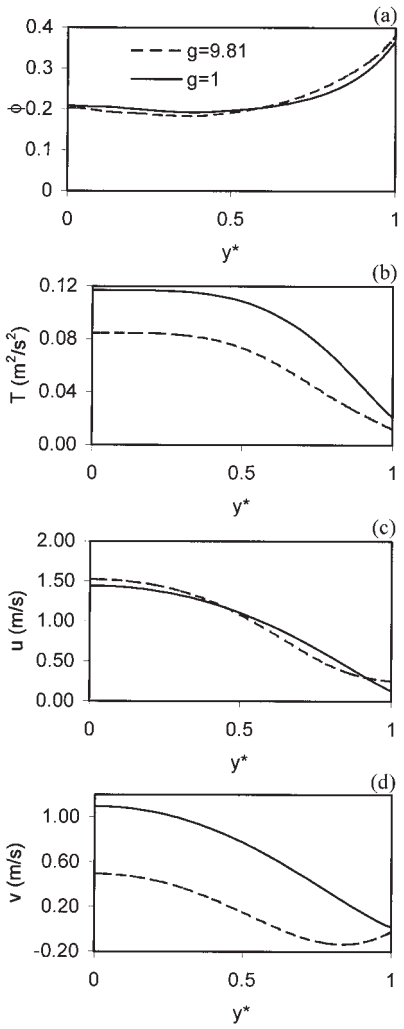

Figure 12. Effect of gravity on gas-particle channel flow for a low gas velocity.

u_g = 1 m/s, e_p = 1, ϕ = 0.22. (a) Solids fraction profile; (b) granular temperature profile; (c) gas velocity profile; (d) solids velocity profile.

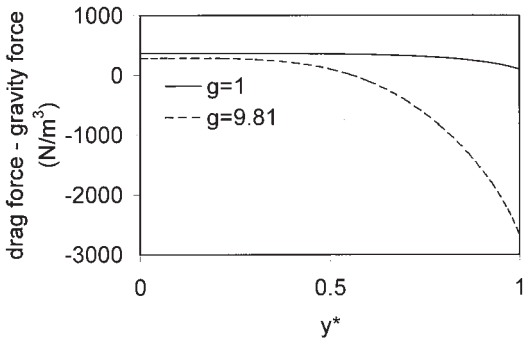

Figure 13. Profiles of drag force minus gravity force across the bed with different gravity.

u_g = 1 m/s, e_p = 1, ϕ = 0.22.

significant as the average gas velocity changes from 10 (see Figure 10) to 1 m/s. When the gravity = 9.81 m/s, the solids flow downward in the region close to the walls, although the average solids velocity = 0.16 m/s. When the gravity decreases to 1 m/s^2, the average solids velocity increases to 0.7 m/s and particles always move upward in the bed. So the particle annular downflow observed in the high gravity situation is no longer present. The difference between the magnitude of the drag force and the magnitude of the gravity force is plotted in Figure 13. In the center the value of the drag force minus gravity force is comparable between the high gravity case and the low gravity case. However, this value decreases rapidly under the high gravity situation when moving toward the walls, whereas this value changes only slightly under the low gravity situation.

Because the drag force plays a key role in the study of the parameter g, an investigation of the effect of different expressions for the drag force was carried out. Here, another correlation adopted by Wen and Yu,[45] Eq. 11, was studied, and the flow profiles based on different gravity values are shown in Figure 14. It can be seen that with a high gas velocity, using Wen and Yu's[45] constitutive relation for the drag force the gas-particle flows are still insensitive to the gravity except that the granular temperature becomes smaller with an increase in gravity. In Figures 10 and 14, the calculations for g = 9.81 m/s^2 were carried out under the same conditions except different drag force expressions. A scrutiny of these two figures indicates that the flow profiles are not sensitive to the expressions of the drag force, which is in agreement with the results from Yasuna et al.[5] When the average gas velocity is decreased, flow profiles similar to those in Figure 12 are obtained with Wen and Yu's constitutive relation for the drag force (not shown). The above observation could be useful for setting up fluidized bed reactors in sites with different gravity values, such as on the Moon and Mars, or centrifugal geometries. However, we would expect that the growth rate of instabilities would vary significantly with gravity. So unsteady-state structures may be rather different.[35]

So far we have considered gas-particle flows only in a narrow system, where the width of the bed is 4 cm. In industry, the width (or diameter) of gas-fluidized beds is normally much larger than this. Therefore, it is of practical importance to extend our calculations to wider systems. The continuation of solids fraction amplitude, $\phi_{max} - \phi_{min}$, as a function of the dimensionless width D (Δ/d) is shown in Figure 15. It is clear that there are two branches in the continuation profile. In the first branch (A–B), initially the solids fraction amplitude increases with an increase of the bed width, after which the increase of the solids fraction amplitude slows down and a plateau curve is observed. As the dimensionless coefficient D increases to 350, the continuation profile switches to the second branch, in which the solids fraction amplitude linearly increases with an increase in the bed width. To better investigate the effect of the bed width on the flow structures, the flow profiles of solids fraction, granular temperature, and gas and solid velocities are plotted for points A, B, and C in Figure 15. For a narrow system, a "core–annular" flow structure is observed, given that elastic particle–particle collisions are assumed. However, with an increase in the bed width, the segregation of particles has a transition from the walls to the center. In branch A–B the solids fraction increases both at the

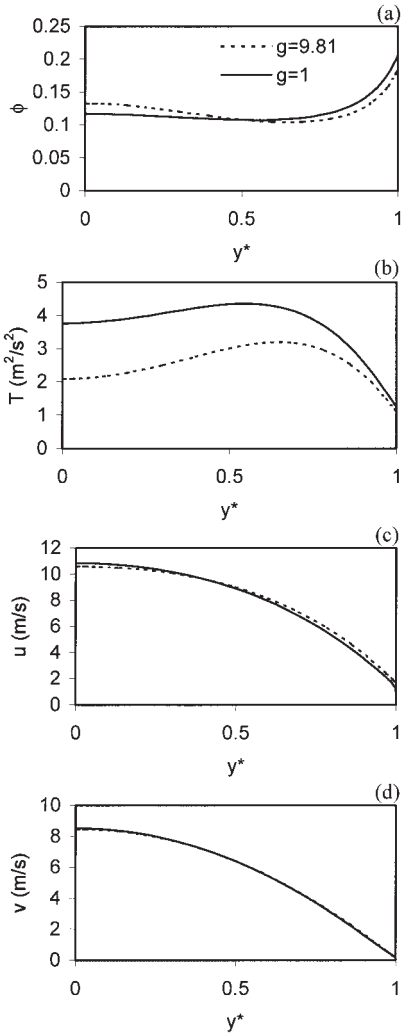

Figure 14. Effect of gravity on gas-particle channel flows with constant gas velocity, using Wen and Yu's correlation[45] for the drag coefficient.

u_g = 8.5 m/s, e_p = 1, ϕ = 0.12. (a) Solids fraction profile; (b) granular temperature profile; (c) gas velocity profile; (d) solid velocity profile.

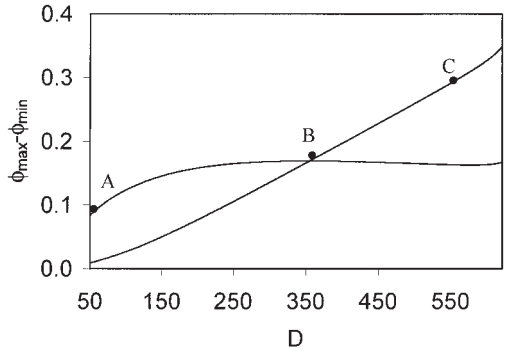

Figure 15. Variation of the solids fraction amplitude, $\phi_{max} - \phi_{min}$, with the dimensionless coefficient D (Δ/d).

$\phi = 0.1$, $e_p = 1$.

walls and at the center with increasing D, and the maximum of the solids fraction is observed at the walls, although the increase in the solids fraction is faster at the center than at the walls. When the value of D is >250, the increase in solids fraction at the walls stops. Thus a plateau curve of solids fraction amplitude is observed. With continuously increasing bed width, the maximum of solids fraction has a transition from the walls to center, and the curve switches to the B–C branch. The increase in the solids fraction at the center has a linear relation with an increase in the bed width. The magnitude of the granular temperature significantly increases with an increase in the bed width as a result of the growth of the gas- and solid-phase velocities when the gas pressure drop is held constant. It is found that the average gas-phase velocity almost linearly increases with an increase in the bed width. Scrutiny of Figures 16c and 16d reveals that in a narrow system the difference of gas and solid velocities at the center is pronounced, whereas with increasing bed width this difference is reduced. This is because in Eq. 14 the gas-particle relative velocity is multiplied by D, leading to a reduction in the relative velocity with an increase in D.

The next parameter considered is the average solids fraction, based on the constraint of Eq. 21. The average solids fraction is changed with a variation of the coefficient C_1 (in Eq. 21) as other physical parameters are hold constant. In the present work, the effect of the average solids fraction is examined by plotting the continuation profile of the variation of the average solids fraction with C_1 because it is not very meaningful to study the solids fraction amplitude if the average solids fraction in the system is different. For a narrow system ($D = 50$), Figure 17 shows that the continuation of average solids fraction has three branches with the variations of C_1. The upper branch indicates that the fluidized bed is almost operated in a packed bed state, whereas the lower branch indicates that the fluidized bed is operated in a relatively low solids concentration state. The curve connecting these two branches represents a series of unstable solutions for the steady state. For a certain range of C_1, three solutions coexist in the system with a same set of physical parameters, whereas the lower one represents a dilute state, the upper one represents a packet bed state, and the middle one denotes an unstable transition state. We find that if C_1 is used as a parameter instead of the average solids fraction

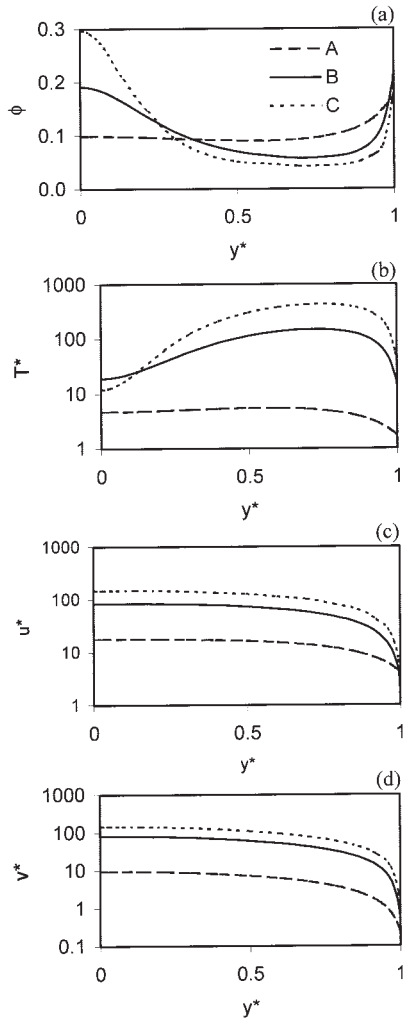

Figure 16. Effects of bed width on gas-particle channel flow.

$\phi = 0.1$, $e_p = 1$. (a) Solids fraction profile; (b) granular temperature profile; (c) gas velocity profile; (d) solid velocity profile (points A, B, and C are given in Figure 15).

in the previous analysis, this "S" curve is a typical continuation profile for narrow gas-fluidized beds with the physical parameters used in the present work. As we track the variations of the

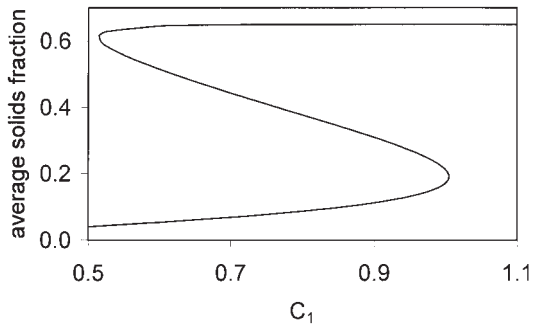

Figure 17. Variations of average solids fraction with the coefficient C_1 in a narrow system.

$e_p = 1$, $D = 50$.

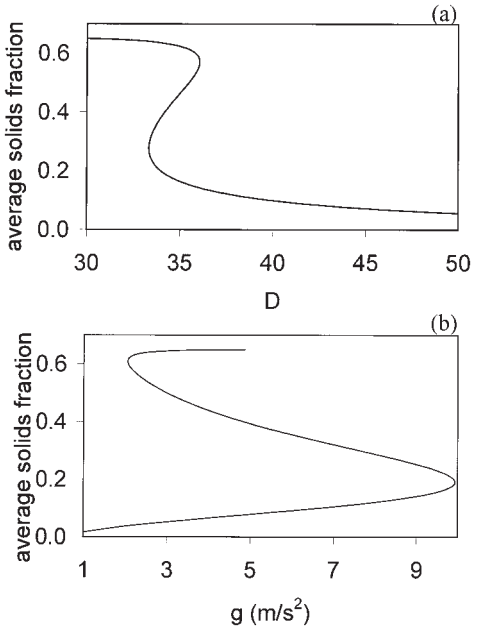

Figure 18. Variations of average solids fraction with physical parameters.

$e_p = 1$, $D = 50$. (a) Effect of the dimensionless coefficient D (Δ/d); (b) effect of gravity.

average solids fraction with D and gravity, respectively, similar continuation curves are obtained (see Figure 18).

When we extend our analysis to a wider system ($D = 500$), two continuation branches coexist in the system. In Figure 19, initially the average solids fraction increases with an increase in C_1. As C_1 passes through a maximum, the solution branch starts to turn back and the average solids fraction increases with a decrease in C_1. The continuation stops in the second branch, and the third branch observed in narrow systems representing the packet bed states is absent here. To better understand the variations of flow profiles with C_1, three points—A, B, and C—are selected from Figure 19, and their solids fraction profiles are plotted in Figure 20. For a low solids fraction state (point A), particles are segregated near the walls and a flat curve is observed at the center. With an increase in average solids fraction, the particle segregation has a transition from the walls to the center. As the average solids fraction increases to

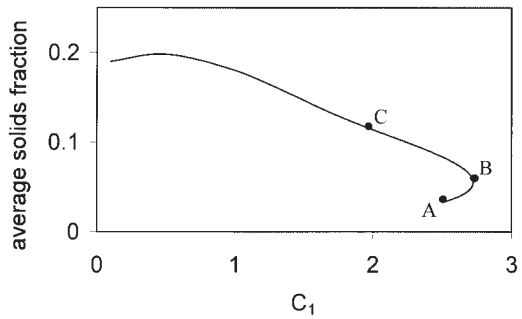

Figure 19. Variations of average solids fraction with the coefficient C_1 in a wide system.

$e_p = 1$, $D = 500$.

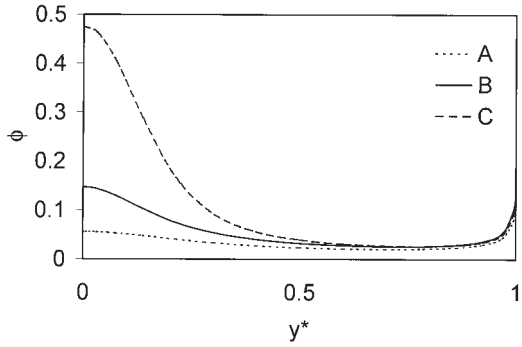

Figure 20. Solids fraction profiles corresponding to points A, B, and C in Figure 19.

$e_p = 1$, $D = 500$.

0.12 (point C), the particle concentration at the center is much higher than that near the walls. Recalling the analysis of the effect of the variation of the bed width, it seems that an increase in the bed width or an increase in the average solids fraction enhances the migration of particles from the walls to the center. Therefore, as e_p is assumed equal to 1, a "core–annular" flow structure can be observed for a very dilute system with high bed width, whereas a core segregation of particles becomes pronounced for a wide system with a moderate solids load, such as when the average solids fraction is >0.05. Reducing e_p just makes the core segregation more pronounced.

The transition from "core–annular" structure to core segregation structure observed in the narrow system when the value of e_p is reduced from 1 cannot be seen in the wide system. Thus the sensitivity to e_p is reduced as the bed width increases. The origin of the transitions observed in Figures 16 and 20 arises from the contribution of gas-particle slip (J_{vis}) on the pseudo-thermal energy transport. By analyzing Eq. 16, it is clear that the contribution of gas-particle slip increases with an increase in the solids fraction, and is greatly enhanced with an increase in the bed width because the dimensionless parameter D is multiplied by the damping contribution term and D^2 is multiplied by the production contribution term. If the gas-particle slip term is not considered in the model, particles are always segregated near the walls when $e_p = 1$ (see Figure 21), and the

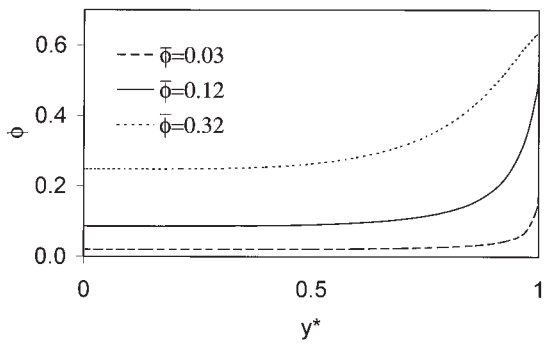

Figure 21. Solids fraction profiles for different average solids fraction when the contribution of gas-particle slip term (J_{vis}) is not considered.

$e_p = 1$, $D = 500$.

bed width and the average solids fraction have only a negligible effect on the transition of particle segregation.

It is useful to examine the sensitivity of these results to different closures to solids-phase stress. One model we have examined was proposed by Sela and Goldhirsch,[59] who used a more accurate calculation approach to obtain solid-phase constitutive relations. In this model, the Boltzmann equation was perturbatively solved, and the constitutive relations were derived by performing a double expansion of the single-particle distribution in the Knudsen number and the degree of inelasticity. In Lun et al.,[20] instead, an ansatz for the form of the single-particle distribution was used to substitute into the Enskog equations. We have solved for gas-particle flow in a channel using the closures of Sela and Goldhirsch.[59] The particle segregation still has a transition from the walls to the center when e_p decreases from 1 to 0.99. Another question that arises is the effect of using an impact velocity–dependent e_p to replace the constant e_p used in the present simulation. However, the closures incorporating an impact velocity–dependent e_p are not easily obtained. To the best of our knowledge, only Lun et al.[60] reported a simple estimation of these terms. In their approximation, the impact velocity is proportional to the square of the granular temperature. Because for slightly inelastic systems only the energy dissipation term in Eq. 5 is sensitive to the variation of e_p, a modified model is established by changing the energy dissipation term based on an impact velocity–dependent e_p, and holding other terms unchanged:

$$J_{coll} = \frac{12\rho_s\phi^2 g_0}{\pi^{1/2}d} C^* T^{3/2}$$

$$C^* = -4\bar{T} + (\pi\bar{T})^{1/2}(3 + 8\bar{T})\exp(4\bar{T})\mathrm{erfc}(2\bar{T}^{1/2}) \qquad (22)$$

where erfc(x) is the usual complementary error function, approximated using rational functions,[61] and the dimensionless $\bar{T}$ is equal to C^*T and the value of C is about (0.005^2) from experimental measurements. We find that the computed solutions are not sensitive to e_p, using this modified model, because the particles always segregate in the center and the "core–annular" flow structure is not observed.

Because the equations have been nondimensionalized in the present work, it is interesting to look at the effects of dimensionless numbers. Generally, two dimensionless numbers are used to classify flow regimes and investigate instabilities in gas-particle fluidized beds. One has a form of Reynolds number (Re), which is equal to B^*D^*E in our model, and the other is the Froude number (Fr), which is equal to $1/C$ in the calculations. It is important to note that here the dimensionless group Re is evaluated by the particle terminal velocity whereas the Reynolds number used to classify flow regimes in gas-fluidized beds is frequently evaluated by the gas-phase velocity. From Figure 22, it can be seen that the steady-state flows are not sensitive to Re. The flow profiles have no difference as Re changes from 2000 to 200 because the viscous term of the gas phase is relatively small in a high Re situation (see Eq. 13) and the flow behavior is independent of Re without this term. With a decrease in Re, the gas viscous term becomes important in Eq. 13, and gas and particle velocities are decreased. The influence of the Froude number is more pronounced (see Figure 23). When the average solids fraction and gas pressure drop are held constant, the gas- and particle-phase velocities decrease with increasing Froude number, leading to a decrease in the granular temperature. When this dimensionless number is high enough, the contribution of the viscous terms for both gas and particle phases can be neglected, and the system can be simplified to a force balance between the gas-particle drag force and the bed gravity force. Because a higher granular temperature means a higher particle pressure and particle viscosity, which can suppress instabilities in gas-particle fluidized beds, a gas-fluidized bed with a lower Froude number is likely to be more stable, which is in agreement with the analysis of Wilhelm and Kwauk.[42]

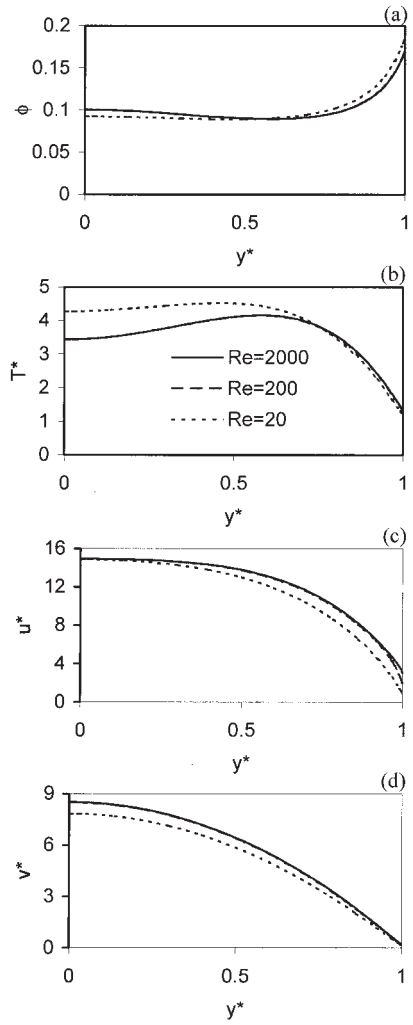

Figure 22. Effects of Reynolds number on gas-particle channel flow.

$\phi = 0.1$. (a) Solids fraction profile; (b) granular temperature profile; (c) gas velocity profile; (d) solid velocity profile.

Conclusion

In this article, a laminar continuum model is presented to describe gas-particle flows in a channel with monodisperse particles. The steady-state solutions, obtained by a numerical method based on orthogonal collocation, exhibit a variety of structures. The effects of physical parameters on the steady-

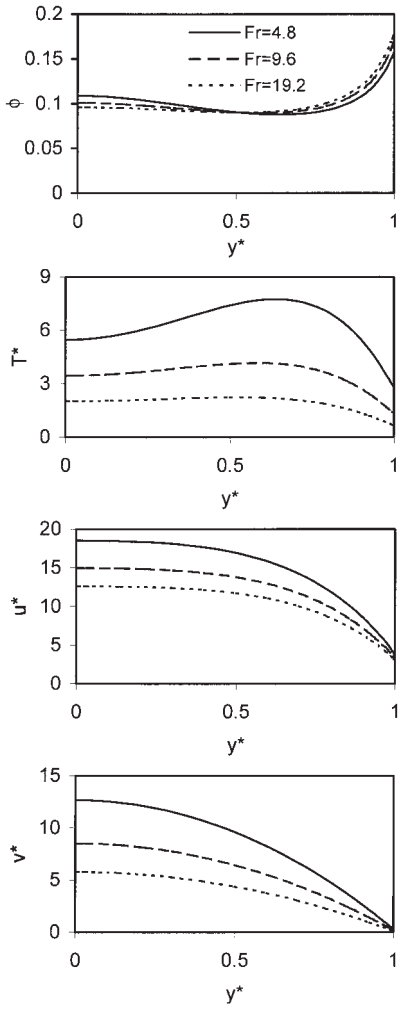

Figure 23. Effects of Froude number on gas-particle channel flow.

$\phi = 0.1$. (a) Solids fraction profile; (b) granular temperature profile; (c) gas velocity profile; (d) solid velocity profile.

state flow profiles were examined, using a continuation approach.

Flow properties are sensitive to the coefficient of particle–particle restitution when its value is close to 1. The particle concentration has a transition from segregation near the walls to segregation at the center when e_p decreases from 1 to 0.99. This sensitivity is reduced when the system becomes more inelastic. A transition in the profiles of particle-phase pressure is also observed with a variation of e_p. The kinetic contribution is small in regions where the collisional contribution is large, and vice versa. In elastic systems, the kinetic pressure has a high level at the center and a low level near the walls. As the system changes from an elastic condition to a slightly inelastic condition, high kinetic pressure switches from the center to the walls.

The second parameter we consider in this paper is gravity. It is found that the continuation diagram corresponding to the variation of the solids fraction amplitude with g is very smooth as g changes more than one order of magnitude. When the pressure drop is held constant, the gas and solid flow rates increase considerably with a decrease in gravity. When the average gas velocity is held constant, the flow profiles are not sensitive to this parameter when the gas velocity is high, which is attributed to the automatic compensation of the gas-particle drag force to the gravitational force. When the gas flow rate is low, however, particles move downward in the region close to the walls with high gravity, whereas this downflow is not observed under a low gravity situation.

In the simulations, it is found that the transition in the solids fraction profiles is not only dependent on the parameter e_p. If e_p is assumed equal to 1, the segregation of particles has the potential to transit from the walls to the center if the gas-particle system changes from a narrow fluidized bed to a wide fluidized bed, or from a dilute fluidized bed to a dense fluidized bed. This transition is explained by the contribution of gas-particle slip on the pseudothermal energy transport. If this term is eliminated, a "core–annular" flow structure is observed as long as the collisions between particles are elastic. In a narrow system, the continuation shows an "S" form bifurcation diagram when we track the variation of the average solids fraction with a certain parameter. However, when we extend our study to wider systems, the upper branch observed in narrow systems representing the packet bed state is absent. Therefore, the continuation diagram has a "U" form. The gas-phase velocity, solid-phase velocity, and pseudothermal temperature greatly increase with increasing bed width.

The effect of two dimensionless numbers has been also studied in the present work. It is found that the flow behavior is not sensitive to the variation of the (terminal velocity based) Reynolds number when this number is high because, under this situation, the contribution of the gas viscous term on the gas-phase momentum balance can be neglected. The effect of the Froude number is more pronounced in our physical situation. The granular temperature is decreased with an increase in the Froude number, as well as the gas and particle velocities.

A goal of work in this area is a full bifurcation and stability analysis (of steady-state and time-dependent solutions) and the results presented in this paper represent a first step in this regard. A linear stability analysis of the steady-state solutions is currently being carried out.

Acknowledgments

This work was partially supported by the National Aeronautics and Space Administration. The authors thank Azzeddine Lekhal for helpful comments.

Notation

d = particle diameter
e_p = coefficient of particle–particle restitution
e_w = coefficient of particle–wall restitution
f = drag force
Fr = Froude number
g = specific gravity force
g_0 = radial distribution function
J_{coll} = dissipation of fluctuational energy through inelastic collisions
J_{vis} = viscous damping and production of fluctuational energy by gas-particle slip
P_f = gas-phase pressure
P_s = solid-phase pressure
q = fluctuational energy flux
Q_g = gas volume flow rate
Q_s = solids volume flow rate
Re = Reynolds number

T = granular temperature
$\underline{u}$ = gas velocity
$\underline{v}$ = solid velocity
$\underline{v}_t$ = solid terminal velocity
x, y = vertical and horizontal directions

Greek letters

β = drag coefficient
2Δ = bed width
ϕ = solids volume fraction
ϕ_{max} = maximum solids volume fraction
φ' = wall specularity coefficient
λ = pseudothermal conductivity
μ = solid-phase viscosity
μ_b = bulk viscosity for particles
μ_g, μ_{eg} = pure and effective gas viscosity
ρ_f = gas density
ρ_s = solid density
$\underline{\underline{\sigma}}_f$ = gas-phase effective stress tensor
$\underline{\underline{\sigma}}_s$ = solid-phase effective stress tensor

Literature Cited

1. Kunii D, Levenspiel O. *Fluidization Engineering*. London, UK: Butterworth-Heinemann; 1991.
2. Sinclair JL, Jackson R. Gas-particle flow in a vertical pipe with particle–particle interactions. *AIChE J*. 1989;35:1473-1486.
3. Pita JA, Sundaresan S. Gas–solid flow in vertical tubes. *AIChE J*. 1991;37:1009-1018.
4. Ocone R, Sundaresan S, Jackson R. Gas-particle flow in a duct of arbitrary inclination with particle–particle interactions. *AIChE J*. 1993; 39:1261-1271.
5. Yasuna JA, Moyer HR, Elliott S, Sinclair JL. Quantitative predictions of gas-particle flow in a vertical pipe with particle–particle interactions. *Power Technol.* 1995;84:23-34.
6. Louge MY, Mastorakos E, Jenkins JT. The role of particle collisions in pneumatic transport. *J Fluid Mech.* 1991;231:345-359.
7. Dasgupta S, Jackson R, Sundaresan S. Turbulent gas-particle flow in vertical risers. *AIChE J*. 1994;40:215-228.
8. Dasgupta S, Jackson R, Sundaresan S. Gas-particle flow in vertical pipes with high mass loading of particles. *Powder Technol.* 1998;116: 190-203.
9. Hrenya CM, Sinclair JL. Effects of particle-phase turbulence in gas-solid flows. *AIChE J*. 1997;43:853-869.
10. Detamore MS, Swanson MA, Frender KR, Hrenya CM. A kinetic-theory analysis of the scale-up of circulating fluidized beds. *Powder Technol.* 2000;110:210-221.
11. Zhang YH, Reese JM. Particle–gas turbulence interactions in a kinetic theory approach to granular flows. *Int J Multiphase Flow* 2001;27: 1945-1964.
12. Helland E, Occelli R, Tadrist L. Numerical study of cluster formation in a gas-particle circulating fluidized bed. *Powder Technol.* 2000;110: 210-221.
13. Goldschmidt MJV, Kuipers JAM, Swaaij WPMV. Hydrodynamic modelling of dense gas-fluidised beds using the kinetic theory of granular flow: Effect of coefficient of restitution on bed dynamics. *Chem Eng Sci.* 2001;56:571-578.
14. Li J, Kuipers JAM. Gas-particle interaction in dense gas-fluidized beds. *Chem Eng Sci.* 2003;58:711-718.
15. Zhou HS, Glamant G, Gauthier D, Lu JD. Lagrangian approach for simulating the gas-particle flow structure in a circulating fluidized bed riser. *Int J Multiphase Flow*. 2002;28:1801-1821.
16. Anderson TB, Jackson R. A fluid mechanical description of fluidized beds. Equations of motion. *Ind Eng Chem Fundam.* 1967;6:527-539.
17. Drew DA. Averaged field equations for two-phase media. *Stud Appl Math.* 1971;50:133-166.
18. Jackson R. Locally averaged equations of motion for a mixture of identical spherical particles and a Newtonian fluid. *Chem Eng Sci.* 1997;52:2457-2469.
19. Wallis GB. The averaged Bernoulli equation and macroscopic equations of motion for the potential flow of a two-phase dispersion. *Int J Multiphase Flow*. 1991;17:683-695.
20. Lun CKK, Savage SB, Jeffrey DJ, Chepurniy N. Kinetic theories for granular flow: Inelastic particles in Couette flow and slightly inelastic particles in a general flow field. *J Fluid Mech.* 1984;140:223-256.
21. Lun CKK. Kinetic theory for granular flow of dense, slightly inelastic, slightly rough spheres. *J Fluid Mech.* 1991;233:539-559.
22. Jenkins JT, Savage SB. A theory for the rapid flow of identical, smooth, nearly elastic, spherical particles. *J Fluid Mech.* 1983;130: 187-202.
23. Jenkins JT, Richman M. Kinetic theory for plane flows of a dense gas of identical, rough, inelastic, circular disks. *Phys Fluids.* 1985;28: 3485-3494.
24. Yerushalmi J, Cankurt N, Geldart D, Liss B. Flow regimes in vertical gas–solid contact system. *AIChE Symp Ser.* 1978;74:1-13.
25. Bader R, Findlay J, Knowlton T. *Circulating Fluidized Bed Technology II*. New York, NY: Pergamon; 1988.
26. Nieuwland JJ, van Sint Annaland M, Kuipers JAM, van Swaaij WPM. Hydrodynamic modelling of gas/particle flows in riser reactors. *AIChE J*. 1996;42:1569-1582.
27. Rhode MJ, Laussmann P. Characterising non-uniformities in gas-particle flow in the riser of a circulating fluidized bed. *Powder Technol.* 1992;72:277-284.
28. Eduardo JB, Yasuna JA, Sinclair JL. Dilute turbulent gas–solid flow in risers with particle–particle interactions. *AIChE J*. 1995;41:1375-1388.
29. Goldhirsch I, Zanetti G. Clustering instability in dissipative gases. *Phys Rev Lett.* 1993;70:1619-1622.
30. Tan ML, Goldhirsch I. Intercluster Interactions in rapid granular shear flows. *Phys Fluids.* 1997;9:856-869.
31. Tan ML, Goldhirsch I. Rapid granular glows as mesoscopic systems. *Phys Rev Lett*. 1998;81:3022-3025.
32. Goldhirsch I. Scales and kinetics of granular flows. *Chaos.* 1999;9: 659-672.
33. Wang CH, Jackson R, Sundaresan S. Stability of bounded rapid shear flows of a granular material. *J Fluid Mech.* 1996;308:31-62.
34. Wang CH, Jackson R, Sundaresan S. Instabilities of fully developed rapid flow of a granular material in a channel. *J Fluid Mech.* 1997; 342:179-197.
35. Gibilaro LG, Foscolo R, Di Felice PU. The influence of gravity on the stability of fluidized beds. *Chem Eng Sci*. 1986;41:2438-2440.
36. Anderson TB, Jackson R. Fluid mechanical description of fluidized beds. Stability of the state of uniform fluidization. *Ind Eng Chem Fundam*. 1968;7:12-21.
37. Jackson R. The mechanics of fluidized beds. I: The stability of the state of uniform fluidization. *Trans IChemE*. 1963;41:13-21.
38. Hirayama O, Tsuzuki T. Linear stability of two-dimensional uniform fluidized beds. *Fluid Dyn Res*. 1995;15:425-435.
39. Anderson K, Sundaresan S, Jackson R. Instabilities and the formation of bubbles in fluidized beds. *J Fluid Mech.* 1995;303:327-366.
40. Glasser BJ, Kevrekidism IG, Sundaresan S. One- and two-dimensional travelling wave solutions in gas fluidized beds. *J Fluid Mech.* 1996; 306:183-221.
41. Glasser BJ, Kevrekidism IG, Sundaresan S. Fully developed travelling wave solutions and bubble formation in fluidized beds. *J Fluid Mech.* 1997;334:157-188.
42. Wilhelm RH, Kwauk M. Fluidization of solid particles. *Chem Eng Prog.* 1948;44:201-218.
43. Agrawal K, Loezos P, Syamlal M, Sundaresan S. The role of meso-scale structures in rapid gas–solid flows. *J Fluid Mech*. 2001;445:151-185.
44. Richardson JF, Zaki WN. Sedimentation and fluidization: Part I. *Trans IChemE*. 1954;32:35-53.
45. Wen CY, Yu HA. Generalized method for predicting the minimum fluidization velocity. *AIChE J*. 1966;12:610-612.
46. Jonnson PC, Jackson R. Frictional-collisional constitutive relations for granular materials, with application to plane shearing. *J Fluid Mech*. 1987;176:67-93.
47. Constantinides A. *Chemical Engineering Series—Applied Numerical Methods with Personal Computers*. New York, NY: McGraw-Hill; 1987.
48. Doedel E, Keller H, Kernevez J. Numerical analysis and control of bifurcation problems. I: Bifurcation in finite dimensions. *Int J Bifurc Chaos* 1991;1:493-520.
49. Miller A, Gidaspow D. Dense, vertical gas-solid flow in a pipe. *AIChE J* 1992;38:1801-1815.
50. Mathiesen V, Solberg T, Hjertager BH. An experimental and compu-

tational study of multiphase flow behavior in a circulating fluidized bed. *Int J Multiphase Flow*. 2000;26:387-419.
51. Benyahia A, Arastoopour H, Knowlton TM, Massah H. Simulation of particles and gas flow behavior in the riser section of a circulating fluidized bed using the kinetic theory approach for the particulate phase. *Powder Technol.* 2000;112:24-33.
52. Foerster SF, Louge MY, Chang H, Allia K. Measurements of the collision properties of small spheres. *Phys Fluids.* 1994;6:1108-1115.
53. Koh CJ, Hookham P, Leal LG. An experimental investigation of concentrated suspension flows in a rectangular channel. *J Fluid Mech*. 1994;266:1-32.
54. Lyon MK, Leal LG. An experimental study of the motion of concentrated suspensions in two-dimensional channel flow. Part 1. Monodisperse systems. *J Fluid Mech.* 1998;363:25-56.
55. Cody GD, Goldfarb DJ, Storch GV, Norris AN. Particle granular temperature in gas fluidized beds. *Powder Technol.* 1996;87:211-232.
56. Poilashenski W, Chen JJC. Normal solid stress in fluidized beds. *Powder Technol.* 1997;90:13-23.
57. Sinclair JL. *Vertical Transport of Gas and Solids with Radial Solid Density Variations*. PhD Dissertation. Princeton, NJ: Princeton University; 1989.
58. Liss ED, Glasser BJ. The influence of clusters on the stress in a sheared granular material. *Powder Technol.* 2001;116:116-132.
59. Sela N, Goldhirsh I. Hydrodynamic equations for rapid flows of smooth inelastic spheres, to Burnette order. *J Fluid Mech*. 1998;361:41-74.
60. Lun CKK, Savage SB, Montreal Q. The effects of an impact velocity dependent coefficient of restitution on stresses developed by sheared granular material. *Acta Mech.* 1986;63:15-44.
61. Abramowitz M, Stegun IA. *Handbook of Mathematical Functions with Formulas, Graphs, and Mathematical Tables* (Applied Math Series 55). Washington, DC: National Bureau of Standards; 1964.

Manuscript received Apr. 5, 2005, and revision received Aug. 23, 2005.